On the Benefit of a Slight PRI Variation for SAR Interferometry

Michelangelo Villano, Nertjana Ustalli, Maxwell Nogueira Peixoto, Josef Mittermayer, Gerhard Krieger, Alberto Moreira
German Aerospace Center (DLR), Microwaves and Radar Institute, Germany

Abstract

Synthetic aperture radar interferometry is a well-established technique for producing high-resolution digital elevation models of the Earth's surface. Observations of some interferograms, however, show that coherent azimuth ambiguities may determine phase biases and coherence losses that significantly degrade the interferometric performance. Whereas imposing very low ambiguity levels may represent a severe design constraint, a slight variation of the pulse repetition interval may suffice decorrelating ambiguities and thus reducing the phase biases and coherence losses without affecting the imaged swath width. This work is relevant for the design of future spaceborne interferometric systems and for the enhanced exploitation of current ones.

1 Introduction

Synthetic aperture radar (SAR) interferometry exploits the coherent combination of two SAR images, acquired from slightly-different viewing angles and often referred to as the master and slave images, to form a digital elevation model (DEM) of the observed scene [1]-[4]. The height accuracy of the resulting DEM ultimately depends on the complex correlation (or coherence) between the two SAR images, which is the product of the contributions of various decorrelation sources, such as thermal noise, quantization noise, baseline decorrelation, volume decorrelation, Doppler decorrelation, temporal decorrelation, coregistration and processing, range and azimuth ambiguities [5]-[6].
Azimuth ambiguities were initially accounted for through a decorrelation contribution $\gamma_{amb,az}$ given by [6]

$$\gamma_{amb,az} = \frac{1}{1 + AASR} \tag{1}$$

where $AASR$ is the azimuth ambiguity-to-signal ratio (AASR), i.e., similarly to thermal noise. Observations of TanDEM-X interferograms, such as the one in **Figure 1** acquired over the Franz Josef Land, Russia, however, have shown that coherent azimuth ambiguities may determine significant interferometric phase biases φ_{bias} and modulations of the coherence magnitude γ, which can be analytically described by the following expressions [7]:

$$\varphi_{bias} = \arg\left\{1 + AASR_{local}\frac{\gamma_a}{\gamma_m}e^{j(\varphi_{0,a}-\varphi_{o,m})}\right\} \tag{2}$$

$$\gamma = \frac{1}{1 + AASR_{local}} \cdot \sqrt{\gamma_m^2 + AASR_{local}^2\gamma_a^2 + 2\,AASR_{local}\frac{\gamma_a}{\gamma_m}\cos\varphi_{0,a} - \varphi_{o,m}} \tag{3}$$

where $AASR_{local}$ is the local azimuth ambiguity-to-signal ratio, γ_m and $\varphi_{o,m}$ are the coherence magnitude and interferometric phase of the ambiguity-free interferogram, and γ_a and $\varphi_{o,a}$ are the coherence magnitude and interferometric phase of the interferogram of the ambiguities.
A spectral-based technique to estimate the local azimuth ambiguity-to-signal ratio is presented in [8], where it is also shown that the latter ratio is likely to be larger than -10 dB in low-backscatter areas and can even reach 0 dB in some cases. As discussed in [9], a local AASR of -5 dB results in a phase bias characterized by a standard deviation of 5 to 10 degrees (depending on the signal-to-noise ratio) and a coherence contribution of azimuth ambiguities in the order of 0.7-0.8, which are critical to be accounted for in the overall coherence budget. One could reduce the local AASR by imposing a lower AASR in the design, but this would drive the complexity and the cost of the SAR system.
The local ambiguity-to-signal ratio could also be reduced by removing azimuth ambiguities through a postprocessing step [10]-[17]. A Wiener filter could be applied, as proposed in [11], but this would result in a resolution degradation, which turns into a reduction of the number of interferometric looks and thus of the coherence. Ambiguities could also be coherently subtracted directly from the interferogram, as first demonstrated in 2011 in a DLR-internal study to reduce the phase errors and coherence loss in the TanDEM-X interferogram of Figure 1 (see also [7], [9]) and then further elaborated for short-baseline along-track interferometry in [18], but the accurate and fully autonomous estimation of the complex scaling coefficient makes this technique challenging.

2 Decorrelating Ambiguities

Equations (2) and (3) suggest that the phase bias and the coherence loss can also be limited by reducing the coherence magnitude of the interferogram of the ambiguities γ_a, i.e., by decorrelating the azimuth ambiguities of the master and slave images. If total decorrelation is achieved, there is no bias anymore and the coherence contribution degenerates into the expression in (1), where $AASR$ has still to be understood as the local one.
γ_a is influenced by the acquisition geometry, which in some cases makes the azimuth ambiguities of the master and slave images be reciprocally shifted and therefore decorrelated. Under the conservative assumption that the acquisition geometry leads to a superposition of the ambiguities, ambiguity decorrelation can still be achieved by acting on the reciprocal sampling of the master and slave images. The repeat-pass and the single-pass cases will be separately discussed in the following.

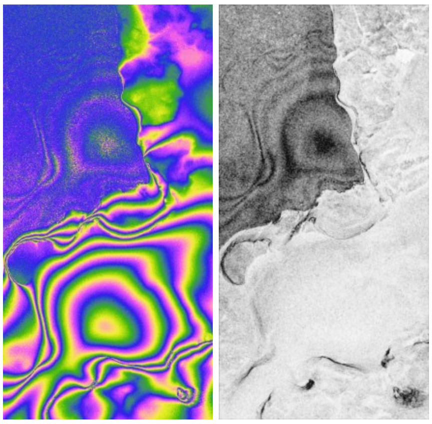

Figure 1 Interferometric phase (left) and magnitude of the complex coherence (right) of a detail of a TanDEM-X interferogram affected by azimuth ambiguities, acquired over the Franz Josef Land, Russia.

3 Repeat-Pass SAR Interferometry

If the master and the slave images are acquired at different times (this also includes the case of the pursuit monostatic mode of TanDEM-X [6], where the time lag between the two acquisitions is in the order of few seconds), the adoption of a slightly different pulse repetition frequency (PRF) in the two acquisitions might suffice to decorrelate azimuth ambiguities.

Let us consider two acquisitions with slightly different PRFs, PRF_1 and PRF_2, and let us define

$$\Delta PRF \doteq PRF_2 - PRF_1 \tag{4}$$

The first-order azimuth ambiguities for the two acquisitions will be relatively displaced in azimuth by a quantity Δx proportional to ΔPRF and given by [19]-[21]

$$\Delta x = \frac{\lambda\, R_0\, \Delta PRF}{2\, v_S} \tag{5}$$

where λ is the wavelength, R_0 is the radar-target distance, and v_S is the satellite speed, and, in order to decorrelate azimuth ambiguities, the relative azimuth shift Δx has to be larger than the autocorrelation length of the ambiguous signals times the satellite speed.

The latter depends on the power spectral density (PSD) of the ambiguous signals, therefore both on the azimuth antenna pattern and the selected PRF. **Figure 2** shows on the left panel the PSDs of the main signal and the first-order left ambiguity for a rectangular antenna with length $L = 4.8$ m, $\lambda = 0.03$ m, and $PRF = 3000$ Hz, and on the right panel the corresponding normalized autocorrelation functions, obtained as inverse Fourier transforms of the PSDs. As it is apparent, due to the shape of the ambiguous spectrum, the autocorrelation length of the ambiguity can be several times (i.e., 2-3 times) larger than that of the main signal, which can be approximately expressed as $L/(2\, v_S)$. The autocorrelation length become smaller for higher PRF, i.e., around 5000 Hz, which are however unlikely to be used within typical acquisitions.

Defining as α the ratio of the autocorrelation lengths of the ambiguity and the main signal, it holds

$$\Delta PRF > \alpha \frac{L\, v_S}{\lambda\, R_0} \tag{6}$$

where conservative values α of least 2-3 should be assumed. For TanDEM-X, $\Delta PRF \cong 4$ Hz is required for $PRF \cong 3000$ Hz, which does not influence the width of the swath to be imaged. **Figure 3** shows the coherence of the ambiguities, as evaluated with a two-dimensional simulation for TanDEM-X with $PRF = 3000$ Hz and different values of ΔPRF, which confirms the results obtained using (6).

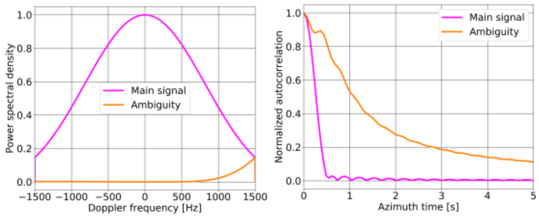

Figure 2 Power spectral densities (left) and normalized autocorrelation functions (right) of the main signal and the first-order left ambiguity for TanDEM-X with $PRF =$ 3000 Hz.

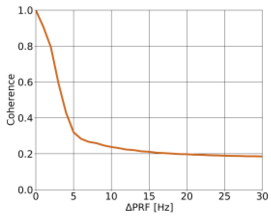

Figure 3 Coherence of the ambiguities for repeat-pass SAR interferometry as a function of the PRF difference between the two acquisition ΔPRF for TanDEM-X with $PRF = 3000$ Hz.

4 Single-Pass SAR Interferometry

If the master and slave images are acquired at the same time and a single transmitter is used, the adoption of a slight, continuous variation of the pulse repetition interval (PRI) could help decorrelate ambiguities, as long as a non-zero along-track baseline B_a is present. The impulse response function (IRF) in proximity of the ambiguities, in fact, is azimuth-variant in case of PRI variation and the along-track baseline induces (after coregistration) a relative azimuth time shift δ_u between the available azimuth samples of the master and slave images roughly given by

$$\delta_u \cong \frac{B_a}{2 v_g} \tag{7}$$

where v_g is the ground velocity and where a bistatic configuration, where the same satellite transmits all pulses has been assumed (**Figure 4**).

Under the assumption that the acquisition geometry leads to a superposition of the ambiguities, the absence of an along-tack baseline leads to the same IRFs of master and slave independently of the PRI variation scheme. At the same time, the presence of an along-track baseline without a PRI variation is not sufficient to avoid the ambiguity correlation, as the ambiguities of the master and slave images might be characterized by different phases, but their phase difference would still be constant (the latter is also the case of **Figure 1**).

In presence of the aforementioned relative shift, the raw data of master and slave could be resampled, e.g., using best linear unbiased (BLU) interpolation [22]-[25], to a uniform grid before focusing and interferogram formation. The coefficients of the BLU interpolation depend on the spectrum of the main signal and are not the optimal ones to resample the ambiguous signal, which will be resampled in a wrong way and, in general, in a different way in the master and slave images, leading to a decorrelation of the ambiguities.

An additional advantage of a PRI variation, especially if followed by a "wrong" resampling, is that ambiguities will be further smeared compared to the constant PRF case and will be therefore characterized by a reduced range resolution. This corresponds to a smaller critical baseline for the ambiguities, which could in turn result in a decorrelation of the ambiguities of distributed scatterers.

Figure 4 Relative azimuth time shift of the samples after co-registration resulting from a non-zero along-track baseline.

4.1 PRI Variation Schemes

The PRI variation scheme will influence the positions of the blind ranges for each range line. In particular, the positions of the blind ranges depend on the moving sum of a number of consecutive PRIs equal to the number of traveling pulses n_t [26], which is roughly given by

$$n_t \cong \frac{2R_0}{c_0 PRI_{mean}} \tag{8}$$

where c_0 is the speed of light.

The continuous variation of the PRI recalls staggered SAR systems, which include BLU interpolation as an integrating part of the concept [22]-[25] and for which ambiguities are likely to be fully smeared and decorrelated [21], [27]. While in staggered SAR, however, a PRI variation is required that ideally shifts blind ranges to all possible positions across the swath in order to have them uniformly distributed, for the scope of this work the PRI variation should allow keeping the width of the imaged swath. Considering that for most SAR systems the imaged swath is smaller than the maximum one allowed by the timing (or diamond) diagram due to e.g., signal-to-noise ratio or ambiguity requirements, a small variation of the blind ranges across the synthetic aperture can be tolerated.

Three PRI variation schemes are considered in the following, namely:

- **Sinusoidal PRI Variation**, whose PRIs can be written as

$$PRI_k = PRI_{mean}\left(1 + A \sin\frac{2\pi k}{N}\right), \quad k = 0,\ N-1 \tag{9}$$

where PRI_{mean} is the mean PRI of the sequence, A is the amplitude of the PRI variation, e.g., $A = 0.01$ means that the PRI variation is ±1% with respect to PRI_{mean}, and N is the length (to be understood as number of PRIs) of the sequence, which repeats then periodically;

- **Square Wave PRI Variation**, whose PRIs can be written as

$$PRI_k = \begin{cases} PRI_{mean}(1+A), k = 0,\ N/2-1 \\ PRI_{mean}(1-A), k = N/2,\ N-1 \end{cases} \tag{10}$$

with N even to keep the symmetry.

- **Random PRI Variation** (to be intended as a sequence of N random PRIs, which repeat periodically), whose PRIs can be written as

$$PRI_k = PRI_{mean}[1 + A\, a_k], k = 0,\ N-1 \tag{11}$$

where a_k is an independent realization of a random variable with uniform distribution between -1 and 1. The advantage of repeating the same sequence of random realizations is justified in 4.2.

Please note that the three PRI variation schemes are expressed so that they are characterized by the same PRI span, if the values of A and N are the same.

4.2 Swath Reduction

If the length N of the sequence of PRIs is much larger than the number of traveling pulses n_t, the maximum achievable swath width W_S for a sinusoidal or a square wave PRI variation is approximately given by

$$W_S \cong (1 - 2\, A\, n_t)W_{S_{const}} \tag{12}$$

where $W_{S_{const}}$ is the maximum swath width obtained for a constant PRI equal to PRI_{mean}, e.g., for $n_t = 16$ and $A = 0.001$, the maximum swath width would reduce by 3.2%, hence the need of keeping the amplitude A very small. The formula is derived under the conservative assumption that the n_t PRIs adjacent to the maximum PRI are all equal to the maximum PRI.

Still under the assumption that the length N of the PRI sequence of PRIs is much larger than the number of traveling pulses n_t, the assessment of the swath reduction for the periodic random PRI variation of (12) cannot be approximated in a straightforward way as in the case of sinusoidal and square wave PRI variations, but requires some further considerations. Due to the randomness of the PRI, theoretically the swath reduction could also reach the value provided in (12), but this worst case would only happen in the very unlikely case that n_t consecutive independent realizations of a_k are all equal or almost equal to 1 (or -1). A more reasonable approach is to resort to probability theory. The sum of n_t PRIs characterized as in (11), i.e., uniformly distributed, follows the Irwin-Hall distribution, which for large values of n_t can be approximated by a Gaussian distribution, whose standard deviation (relative to PRI_{mean}) σ is given by $A\sqrt{n_t}/\sqrt{3}$. By considering an interval of $\pm 2\sigma$ (95% rule) and approximating, we obtain the following expression for the maximum achievable swath width W_S, which looks, but for a square root, very similar to (12):

$$W_S \cong \left(1 - \frac{4}{\sqrt{3}}\, A\sqrt{n_t}\right) W_{S_{const}} \approx (1 - 2\, A\sqrt{n_t})W_{S_{const}} \tag{13}$$

The comparison of (13) to (12) highlights that for a random PRI variation the same swath reduction is obtained for a much larger PRI span (i.e., 4 time larger for $n_t = 16$) compared to the sinusoidal and square wave cases. This is shown with an example in **Figure 5**, which refers to a TanDEM-X like system characterized by a pulse width of 25 µs and a mean pulse repetition interval $PRI_{mean} = 0.303$ ms. The areas in black include not only the blind ranges in the raw data, but also areas characterized by reduced range resolution after pulse compression [23]-[24].

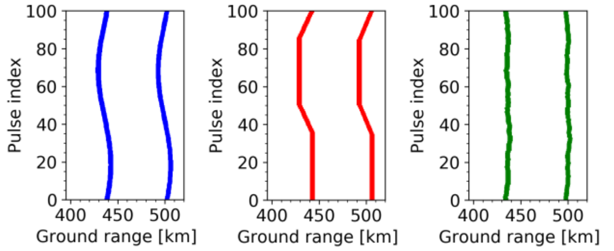

Figure 5 Swath decrease at a slant range around $R_0 = 700$ km as a result of the sinusoidal PRI variation in (9) with $N = 100$ and $A = 0.007$ (left), the square wave PRI variation of (10) with $N = 100$ and $A = 0.007$ (center) and a random PRI variation of (11) with $N = 100$ and $A = 0.007\sqrt{n_t}$ (right).

A larger PRI span implies a further smearing of azimuth ambiguities, which might help reducing the critical baseline, as discussed above. The interval has been chosen around $\pm 2\sigma$ and not larger, because the length of the PRI sequence is limited and so is the number of realizations – this justifies repeating the same random sequence rather than having a very long one (requirements on the minimum PRI sequence length will be discussed in 4.3) – and assuming that an “unfortunate” realization can just be discarded, as the system designer can choose the PRI variation to be adopted for the acquisition in advance.

If the length of the PRI sequence N is instead equal to the number of traveling pulses n_t (or to $n_t - 1$), larger PRI span (and namely amplitudes A) can be exploited without incurring in a significant swath reduction. For all three considered PRI variations, in fact, the moving sum will be constant for one of the two blind ranges delimiting the swath, due to the fact that the addends of the moving sum stay the same, and almost constant for the other one, where the moving sum includes $N - 1$ out of the N values. In this case for all three considered PRI variations the same PRI span leads to the same swath reduction and the maximum achievable swath width W_S can be approximated as

$$W_S \cong (1 - A) W_{S_{const}} \tag{14}$$

In this case, in fact, the maximum relative variation of the blind range is $2A$ (i.e., the highest possible difference between 2 PRIs of the sequence), but the swath reduction is only due to one of the two blind ranges.

Figure 6 shows an example of the case $N = n_t$ for the three considered PRI variations. It is apparent that the swath reduction is much smaller than in Figure 4, although the PRI span is much larger ($A = 0.05$ vs. $A = 0.007$). For $N = n_t - 1$, the moving sum would be constant for the closer of the two blind ranges and (14) will still hold.

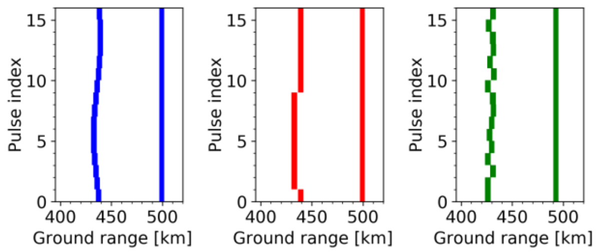

Figure 6 Swath decrease for the case $N = n_t = 16$ at a slant range around $R_0 = 700$ km as a result of the sinusoidal PRI variation in (9) (left), the square wave PRI variation of (10) (center) and a random PRI variation of (11), all with $A = 0.05$.

4.3 Decorrelation and Along-Track Baseline

The PRI variation scheme and its parameters N and A have to be selected for a given along-track baseline in order to provide a substantial decorrelation of azimuth ambiguities, while keeping the swath reduction as small as possible.

The trend of ambiguity decorrelation versus along-track baseline can be obtained for a specific set of system parameters and an along-track baseline by means of simulation. For a periodic PRI sequence, this trend will also be periodic with period $B_{a_{period}}$ given by

$$B_{a_{period}} = 2\, v_g \sum_{k=0}^{N-1} PRI_k \cong 2\, v_g\, N\, PRI_{mean} \tag{15}$$

This means that for an along-track baseline equal to integer multiples of $B_{a_{period}}$ the samples of master and slave in spite of the PRI variation and the non-zero along-track baseline will still be available at the same positions and will not determine any ambiguity decorrelation.

Given a sequence of PRI and an along-track baseline, it is possible to assess the resulting ambiguity decorrelation by convolving the impulse response of the ambiguity, which is in general different for the master and slave images, with fully-developed speckle and estimating the coherence. For sinusoidal and square wave PRI variations, it can be observed that the coherence of the ambiguities decreases as the along-track baseline increases from 0 to $B_{a_{period}}/2$ (or from $p\, B_{a_{period}}$ to $p\, B_{a_{period}} + B_{a_{period}}/2$, with $p \in \mathbb{N}$), as the relative shift between the available samples of master and slave increases. Likewise, as the along-track baseline increases from $B_{a_{period}}/2$ to $B_{a_{period}}$ (or from $p\, B_{a_{period}} + B_{a_{period}}/2$ to $(p+1) B_{a_{period}}$, with $p \in \mathbb{N}$), the coherence of the ambiguities increases. The maximum decorrelation therefore occurs for

$$B_a = (p + 1/2) B_{a_{period}}, p \in \mathbb{N} \tag{16}$$

where $\mathbb{N}$ also include 0. For random PRI variations the along-track baseline that leads to the maximum ambiguity decorrelation depends on the specific PRI realizations, still the minimum usually corresponds to the value of B_a given in (16).

These considerations therefore suggest that the length N of the PRI sequence can be selected (at least for sinusoidal and square wave schemes) so that the maximum decorrelation is obtained. By substituting (15) in (16) it holds

$$N \cong \frac{B_a}{2\,(p + 1/2)\, v_g\, PRI_{mean}}, p \in \mathbb{N} \tag{17}$$

The expression in (21) provides a set of possible values of N, that can be obtained by varying the integer variable p and, if needed, to some extend the value of PRI_{mean}, assuming that B_a and v_g are given. For $B_a = 290$ m, $v_g = 7040$ m/s and $PRI_{mean} = 0.303$ ms, for instance, we can choose $N = 136$ (corresponding to $p = 0$ and belonging to the case $N \gg n_t$), but also $N = 16$ (corresponding to $p = 4$ and belonging to the case $N = n_t$) or other further values of N.

Once different options for the sequence length are available, the parameter A, related to the PRI span, needs to be selected. In general, the higher the PRI span, the more substantial the ambiguity decorrelation, but also the more significant the swath reduction.

Two-dimensional (2-D) simulations have been carried out for a typical spaceborne scenario and the same sequences for which the swath reduction had been assessed in Figure 5 and Figure 6. The coherence has been estimated using a 9×9-pixel window. **Figure 7** shows for the aforementioned PRI variations the coherence of the ambiguities as a function of the along-track baseline. These plots have to be considered as periodical, i.e., they repeat with a period given by the maximum along-track baseline given in the plot.

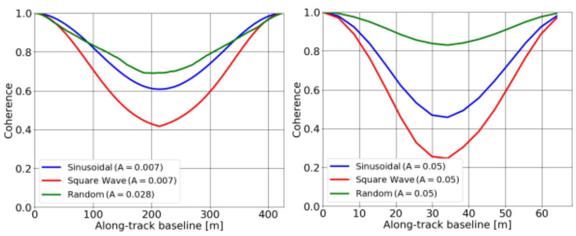

(a) (b)

Figure 7 Coherence of the ambiguities as a function of the along-track baseline for the sinusoidal PRI variation in (9) (blue), the square wave PRI variation of (10) (red) and the random PRI variation of (11) (green). (a) $N = 100$ (length of the sequence of PRIs is much larger than the number of traveling pulses), corresponding to swath width reduction depicted in Figure 5. (b) $N = 16$ sinusoidal PRI variation (length of the sequence of PRIs equal to the number of traveling pulses), corresponding to swath width reduction depicted in Figure 6.

It can be noticed that long sequences allow decorrelation for larger along-track baselines, although one could also exploit in some cases the periodical effect with short sequences. Figure 5 (c) shows that for a short sequence and a small amplitude the achieved decorrelation might not be enough.

As is apparent for comparable swath reduction, the square wave PRI variation allows in both cases for the highest decorrelation, while a random PRI variation is less effective, especially if the length of the sequence of PRIs is equal to the number of traveling pulses.

5 Impact on Interferogram and DEM Quality

In order to observe the impact of ambiguity decorrelation on the interferogram and the resulting DEM for different level of coherence, simulated interferograms and DEM have been generated starting from the dataset of Figure 1. In particular, after removing the azimuth ambiguities from both master and slave using a Wiener filter, the ambiguities have been re-introduced by convolving the main response with the IRF of the ambiguity, translating and scaling it. Furthermore, different degrees of coherence of the ambiguity have been introduced. Figure 8 shows the resulting interferometric phase, coherence, and DEM, for a system with *AASR* = -17 dB, in both the case of no decorrelation and that of a coherence of the interferogram of ambiguities equal to 0.3.

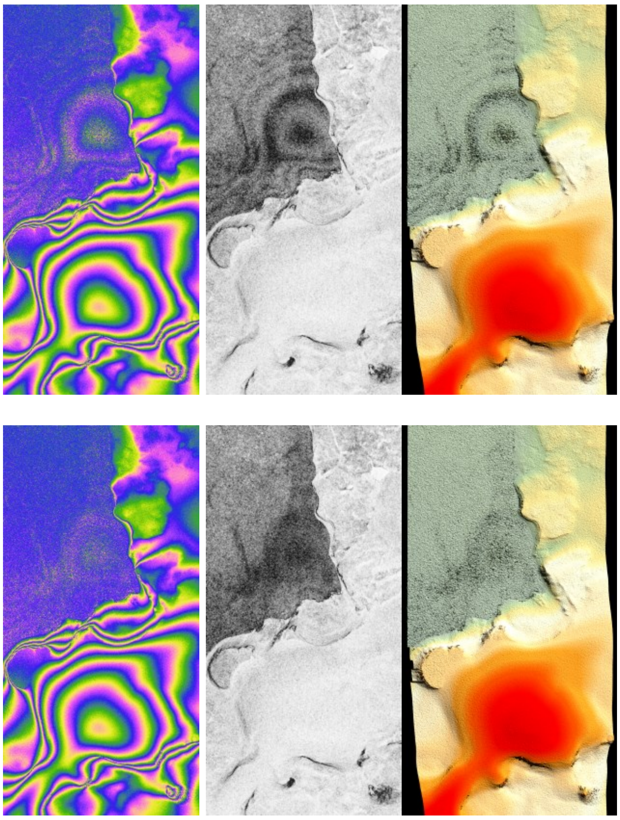

Figure 8 Impact of ambiguity decorrelation on interferometric phase (left), interferometric coherence (center), and DEM (right). (top) No decorrelation. (bottom) Coherence of the ambiguity = 0.3.

6 Conclusions and Outlook

This paper proposes a method to decorrelate azimuth ambiguities in SAR interferometry through a slight variation of the PRI either between the two acquisitions (for the repeat-pass case) or in a continuous periodic way (for the single-pass case). The PRI variation scheme needs to account for the along-track baseline of the acquisition and to be optimized accordingly. While an accurate performance assessment can only be performed for a specific system, simple simulations under conservative assumptions show the potential of the technique, which could be useful for the design of future spaceborne interferometric systems, such as High Resolution Wide Swath (HRWS) [28], as well as for the enhanced exploitation of current ones.

7 Literature

[1] R. Bamler and P. Hartl, "Synthetic aperture radar interferometry," *Inv. Probl.*, vol. 14, no. 4, pp. R1–R54, Feb. 1998.

[2] P. A. Rosen *et al*., "Synthetic aperture radar interferometry," *Proc. IEEE*, vol. 88, no. 3, pp. 333-382, March 2000.

[3] R. F. Hanssen, *Radar interferometry: data interpretation and error analysis*, Springer, Dordrecht, The Netherlands, 2001.

[4] A. Moreira, P. Prats-Iraola, M. Younis, G. Krieger, I. Hajnsek and K. P. Papathanassiou, "A tutorial on synthetic aperture radar," *IEEE Geosci. Rem. Sens. Mag.*, vol. 1, no. 1, pp. 6-43, March 2013.

[5] H. A. Zebker and J. Villasenor, "Decorrelation in interferometric radar echoes," *IEEE Trans. Geosci. Rem. Sens.*, vol. 30, no. 5, pp. 950-959, Sept. 1992.

[6] G. Krieger, A. Moreira, H. Fiedler, I. Hajnsek, M. Werner, M. Younis, and M. Zink, "TanDEM-X: A satellite formation for high-resolution SAR interferometry," *IEEE Trans. Geosci. Remote Sens.,* vol. 45, no. 11, pp. 3317–3341, Nov. 2007.

[7] M. Villano and G. Krieger, "Impact of Azimuth Ambiguities on Interferometric Performance," *IEEE Geosci. Rem. Sens. Lett.*, vol. 9, no. 5, pp. 896-900, Sept. 2012.

[8] M. Villano and G. Krieger, "Spectral-Based Estimation of the Local Azimuth Ambiguity-to-Signal Ratio in SAR Images," *IEEE Trans. Geosci. Remote Sens.*, vol. 52, no. 5, pp. 2304-2313, May 2014.

[9] M. Villano and G. Krieger, "Accounting for azimuth ambiguities in interferometric performance analysis," *2012 IEEE Int. Geosci. Rem. Sens. Symposium*, 2012.

[10] A. Moreira, "Suppressing the azimuth ambiguities in synthetic aperture radar images," *IEEE Trans. Geosci. Remote Sens.*, vol. 31, no. 4, pp. 885-895, July 1993.

[11] A. Monti Guarnieri, "Adaptive removal of azimuth ambiguities in SAR images," *IEEE Trans. Geosci. Remote Sens.*, vol. 43, no. 3, pp. 625–633, Mar. 2005.

[12] Z. Yu and M. Liu, "Suppressing azimuth ambiguity in spaceborne SAR images based on compressed sensing," *Science China Information Sciences*, vol. 55, no. 8, pp. 1830-1837, 2012.

[13] M. Liu, Z. Yu, and C. Li, "Azimuth ambiguity suppression for spaceborne SAR based on PRF microvariation," *2013 IEEE Int. Geosci. and Rem. Sens. Symposium*, 2013.

[14] J. Chen, M. Iqbal, W. Yang, P. Wang, and B. Sun, "Mitigation of azimuth ambiguities in spaceborne stripmap SAR images using selective restoration," *IEEE Trans. Geosci. Remote Sens.*, vol. 52, no. 7, pp. 4038–4045, Jul. 2014.

[15] G. Di Martino, A. Iodice, D. Riccio, and G. Ruello, "Filtering of azimuth ambiguity in stripmap synthetic aperture radar images," *IEEE J. Sel. Top. Appl. Earth Obs. Rem. Sens.*, vol. 7, no. 9, pp. 3967-3978, 2014.

[16] J. Chen, K. Wang, W. Yang, and W. Liu, "Accurate reconstruction and suppression for azimuth ambiguities in spaceborne stripmap SAR images," *IEEE Geosci. Rem. Sens. Lett.*, vol. 14, no. 1, pp. 102-106, 2016.

[17] Y. Long, F. Zhao, M. Zheng, G. Jin, and H. Zhang, "An azimuth ambiguity suppression method based on local azimuth ambiguity-to-signal ratio estimation," *IEEE Geosci. Rem. Sens. Lett.*, vol. 17, no. 12, pp. 2075-2079, 2020.

[18] P. López-Dekker, Y. Li, L. Iannini, P. Prats-Iraola and M. Rodríguez-Cassola, "On Azimuth Ambiguities Suppression for Short-Baseline Along-Track Interferometry: the Stereoid Case," *2019 IEEE Int. Geosci. Rem. Sens. Symposium*, 2019, pp. 110-113.

[19] F. K. Li and W. T. K. Johnson, "Ambiguities in spaceborne synthetic aperture radar systems," *IEEE Trans. Aerosp. Electron. Syst.*, vol. 19, no. 3, pp. 389–397, May 1983.

[20] R. K. Raney and G. J. Princz, "Reconsideration of Azimuth Ambiguities in SAR," *IEEE Trans. Geosci. Remote Sens.*, vol. GE-25, no. 6, pp. 783-787, Nov. 1987.

[21] N. Ustalli and M. Villano, "Impact of Ambiguity Statistics on Information Retrieval for Conventional and Novel SAR Modes," *2020 IEEE Radar Conf.*, 2020, pp. 1-6.

[22] M. Villano, G. Krieger, and A. Moreira, "Staggered SAR: High-Resolution Wide-Swath Imaging by Continuous PRI Variation," *IEEE Trans. Geosci. Remote Sens.*, vol. 52, no. 7, pp. 4462–4479, July 2014.

[23] M. Villano, G. Krieger, and A. Moreira, "A Novel Processing Strategy for Staggered SAR," *IEEE Geosci. Rem. Sens. Lett.*, vol. 11, no. 11, pp. 1891–1895, November 2014.

[24] M. Villano, "Staggered Synthetic Aperture Radar," PhD Thesis, Karlsruhe Institute of Technology, DLR-Forschungsbericht 2016-16, ISSN 1434-8454, Wessling, Germany, 2016.

[25] M. Villano, G. Krieger, M. Jäger, and A. Moreira, "Staggered SAR: Performance Analysis and Experiments with Real Data," *IEEE Trans. Geosci. Remote Sens.*, vol. 55, no. 11, pp. 6617-6638, Nov. 2017.

[26] M. Villano and M. N. Peixoto, "Characterization of Nadir Echoes in Multiple-Elevation-Beam SAR with Constant and Variable Pulse Repetition Interval," *IEEE Trans. Geosci. Remote Sens.*, vol. 60, 2022

[27] M. Villano, M. Nogueira Peixoto, N. Ustalli, G. Krieger and A. Moreira, "Staggered SAR: Recent Advances and Design Trade-Offs," *EUSAR 2021*, 2021.

[28] J. Mittermayer et al., "MirrorSAR: An HRWS Add-On for Single-Pass Multi-Baseline SAR Interferometry," *IEEE Trans. Geosci. Remote Sens.*, vol. 60, 2022.